On the evolutionary behaviour of BL Lac objects

Bade, N.; Beckmann, V.; Douglas, N. G.; Barthel, P. D.; Engels, D.; Cordis, L. Nass; Voges, W.

Published in:
Astronomy & astrophysics

Publication date:
1998

A&A manuscript no.
(will be inserted by hand later)

Your thesaurus codes are:
03 (11.01.2; 11.02.1; 13.25.2)

ASTRONOMY AND ASTROPHYSICS

On the evolutionary behaviour of BL Lac objects⋆

N. Bade[1], V. Beckmann[1], N.G. Douglas[2], P. D. Barthel[2], D. Engels[1], L. Cordis[1], P. Nass[3], and W. Voges[3]

[1] Hamburger Sternwarte, Gojenbergsweg 112, D-21029 Hamburg, Germany
[2] Kapteyn Astronomical Institute, P.O.Box 800, 9700 AV Groningen, The Netherlands
[3] MPI für Extraterrestrische Physik, D-85740 Garching, Germany

Received date; accepted date

Abstract. We present a new well defined sample of BL Lac objects selected from the ROSAT All-Sky Survey (RASS). The sample consists of 39 objects with 35 forming a flux limited sample down to $f_X(0.5-2.0\,\mathrm{keV}) = 8 \cdot 10^{-13}\,\mathrm{ergs\,cm^{-2}\,s^{-1}}$, redshifts are known for 33 objects (and 31 of the complete sample). X-ray spectral properties were determined for each object individually with the RASS data. The luminosity function of RASS selected BL Lac objects is compatible with results provided by objects selected with the *Einstein* observatory, but the RASS selected sample contains objects with luminosities at least tenfold higher. Our analysis confirms the negative evolution for X-ray selected BL Lac objects found in a sample by the *Einstein* observatory, the parameterization provides similar results. A subdivision of the sample into halves according to the X-ray to optical flux ratio yielded unexpected results. The extremely X-ray dominated objects have higher redshifts and X-ray luminosities and only this subgroup shows clear signs of strong negative evolution. The evolutionary behaviour of objects with an intermediate spectral energy distribution between X-ray and radio dominated is compatible with no evolution at all. Consequences for unified schemes of X-ray and radio selected BL Lac objects are discussed. We suggest that the intermediate BL Lac objects are the basic BL Lac population. The distinction between the two subgroups can be explained if extreme X-ray dominated BL Lac objects are observed in a state of enhanced X-ray activity.

Key words: galaxies: active - BL Lacertae objects: general - X-rays: galaxies

1. Introduction

The most common view about BL Lac Objects is that we are looking into a highly relativistic jet (Blandford & Rees, 1978). The high variability, the polarization, and the spectral energy distribution can in principle all be explained with this model. But there are still unsolved problems for this model. Examples are the nature of the mechanism(s) that generates and collimates the jet. The evolution of physical parameters as the energy and momentum density along the jet is not yet clear, too. An important question is also whether the jets are composed of highly relativistic hadronic or leptonic plasma (Kollgaard, 1994). Furthermore there exists the competing theory that at least some BL Lac objects originate from microlensed QSO (Ostriker & Vietri, 1985). Models of BL Lac objects must explain why X-ray and radio selected BL Lac objects differ in some observational characteristics (degree of variability and polarization (Jannuzi et al., 1994)) so that it is not necessarily true that both object classes are of the same astrophysical origin. A sensitive test for the models is the cosmological evolutionary behaviour.

To evaluate the luminosity function and evolution behaviour of an object class complete samples with known distances of each individual object are necessary. For BL Lac objects two problems exist which render the determination of their luminosity function difficult. First, on account of the inconspicuous optical spectral properties of BL Lacs (the absence of strong emission and absorption lines being one of the defining criteria) more effort is required in their selection than is the case with most other object classes. Although there are defining criteria suitable for optical selection (variability, polarisation) no optically selected sample of BL Lac objects with more than 10 objects exists (Kollgaard, 1994). Second, their redshifts are difficult to determine for the same reason.

As a consequence, flux limited samples of BL Lac objects with nearly complete redshift information are rare. Stickel et al. (1991) selected a sample of 35 objects in the radio wavelength region with radio fluxes above 1 Jy. They found a flat redshift distribution between $0.1 < z < 1.2$ and their analysis of the sample revealed positive evolution; radio selected BL Lac objects are more numerous in cosmological distances than in our local neighbourhood. At X-ray wavelengths a com-

Send offprint requests to: N. Bade; e–mail: nbade@hs.uni-hamburg.de

⋆ Based on observations from the German-Spanish Astronomical Center, Calar Alto, operated jointly by the Max-Planck-Institut für Astronomie, Heidelberg, and the Spanish National Commission for Astronomy, and from the William Herschel Telescope operated on the island of La Palma by the Royal Greenwich Observatory in the Spanish Observatorio del Roque de los Muchachos of the Instituto de Astrofísica de Canarias

plete well defined sample was built up with the EMSS (Stocke et al., 1991). Morris et al. (1991) presented a sample of 22 objects down to $f_X(0.3-3.5\,\mathrm{keV}) = 5\cdot10^{-13}\,\mathrm{ergs\,cm^{-2}\,s^{-1}}$, which was later expanded to 30 objects and lower fluxes by Wolter et al. (1994). The EMSS objects exhibit a redshift distribution with strong concentration to low redshifts $\mathrm{z} < 0.3$ and the sample shows clear signs for negative evolution. The EMSS sample was constructed with serendipitously found BL Lac objects from pointed observations of the *Einstein* satellite. Because most these pointed observations were of short exposure, objects with low fluxes are less frequent and are rare in the sample.

We contribute to this discussion with a new sample consisting of 39 X-ray selected BL Lac objects with redshifts available for more than 80% of them. The selection is based on the ROSAT All-Sky Survey (RASS, Voges et al., 1996). With a flux limit of $f_X(0.5-2.0\,\mathrm{keV}) = 8\cdot10^{-13}\,\mathrm{ergs\,cm^{-2}\,s^{-1}}$ and redshifts up to $\mathrm{z}\sim0.8$ the sample is suitable to test the evolutionary behaviour of the sample and to determine the luminosity function of RASS selected BL Lac objects. In an earlier paper (Nass et al., 1996) we presented a larger sample to discuss selection processes of BL Lac objects within the RASS, but we could not deal with the evolutionary behaviour because the flux limit was not deep enough and many redshifts were unknown. The new sample consists of objects with a wide range of spectral energy distributions, from extremely X-ray dominated objects to objects with intermediate spectral energy distribution. Objects with a maximum of νf_ν in the radio or mm wavelength region, which are frequently found among the 1 Jy sample, are not contained in our X-ray flux limited sample. We were able to subdivide the sample into two subgroups according to α_{OX}[1]. Several properties are different in these subgroups.

The following section describes the observational characteristics of the sample in the radio-, optical- and X-ray region. Details of the redshift determination are discussed, bcause it is a delicate process for BL Lac objects. Section III analyses the properties of the sample, in particular the luminosity function and the evolutionary behaviour. In Sect. IV the new results are discussed in the context of unified schemes for BL Lac objects. Several new objects need comments to their redshift determination which are presented in an appendix.

We use cosmological parameters $\mathrm{H_0} = 50\,\mathrm{km\,s^{-1}\,Mpc^{-1}}$ and $q_0 = 0$ in this paper.

2. Observational basis

2.1. Sample and object definition

The sample of BL Lac objects presented here is a subset of the Hamburg ROSAT X-ray bright sample (HRX, Cordis et al., 1996) of AGN. The HRX was pre-identified on direct and objective prism plates which were taken with the Hamburg Schmidt telescope on Calar Alto / Spain within the Hamburg Quasar Survey (HQS, Hagen et al., 1995). Obvious galactic counterparts were excluded from further study (Bade et al., 1997). Slit spectroscopy was performed in order to obtain reliable classifications of the sources unidentified on the Schmidt plates and to determine redshifts for the AGN candidates. Galaxy clusters are not subject of the HRX and they have not been investigated in detail up to now.

[1] we define α_{OX} as the power law index between 1 keV and 4400 Å with $\mathrm{f}_\nu \propto \nu^{-\alpha_{\mathrm{OX}}}$

Table 1. Field boundaries for the surveyed areas with $\delta < 45\,^\circ$. They are complete down to a hard ROSAT PSPC countrate of $0.15\,\mathrm{cts\,s^{-1}}$

R.A.$_{min}$	R.A.$_{max}$	Decl.$_{min}$	Decl.$_{max}$
08h 45m	09 h30m	$19\,^\circ53'$	$25\,^\circ00'$
15h 55m	16 h18m	$19\,^\circ57'$	$25\,^\circ00'$
07h 33m	13 h51m	$25\,^\circ00'$	$30\,^\circ00'$
16h 01m	17 h33m	$25\,^\circ00'$	$30\,^\circ00'$
07h 32m	13 h44m	$30\,^\circ00'$	$35\,^\circ20'$
16h 02m	17 h37m	$30\,^\circ00'$	$35\,^\circ14'$
16h 20m	16 h49m	$39\,^\circ54'$	$45\,^\circ00'$

The sample is drawn from two subareas of the HRX. The area with $45\,^\circ < \delta < 70\,^\circ$ and $8\mathrm{h} < \alpha < 17\mathrm{h}$ covers 1687 deg^2 and it is completely identified down to a hard ROSAT PSPC (0.5 − 2.0 keV) countrate of $0.075\,\mathrm{cts\,s^{-1}}$(corresponding to $\mathrm{f_x}(0.5-2.0\,\mathrm{keV}) = 8\cdot10^{-13}\,\mathrm{ergs\,cm^{-2}\,s^{-1}}$). A detailed description of this core HRX area can be found in an accompanying paper (Cordis et al., in preparation) which also provides identifications for all X-ray sources in this region. A second area with $\delta < 45\,^\circ$ was added for this paper and covers 1150 deg^2. It is complete down to a hard countrate of $0.15\,\mathrm{cts\,s^{-1}}$. Table 1 presents the boundaries of this patchy area.

Table 2 presents BL Lac objects located inside the HRX areas. For the calculation of the luminosity function we restricted ourselves to objects with the above given countrate limits. Their names are marked with an asterisk. In previous identification projects BL Lac objects were more frequent among the last unidentified X-ray sources. Only one X-ray source remained unidentified because we did not take a spectrum from this object. Since the HRX comprises 302 X-ray sources (among them 201 extragalactic sources) this means a completeness level of 99.7%. Selection effects which could be introduced by our identification process are discussed in Sect. 3.

Our criteria to classify X-ray sources as BL Lac objects are essentially spectroscopically similar to the work of the EMSS. By definition the spectra of BL Lac objects are dominated by a nonthermal continuum. Explicitly the selection criteria are:

- Emission lines with $\mathrm{W}_\lambda > 5$Å must be absent.
- The contrast of the Ca II break from the hosting galaxy must be less than 25% in the optical spectrum.

The gathered radio data supported us in selecting our BL Lac candidates, but we did not use radio data to exclude objects from our list of candidates. We did not measure the polarization and did not check the optical variability behaviour of the newly presented objects up to now. Detailed studies of the

EMSS BL Lac objects have shown that X-ray sources with the above mentioned selection criteria are all radio sources (Stocke et al., 1990) and most of them are variable and the duty cycle of polarized emission (fraction of time spent with the degree of polarization greater than 4%) is 44% (Jannuzi et al., 1994).

2.2. Radio properties

Up to now the presented sample was not observed with dedicated radio observations. Nevertheless radio properties of BL Lac objects are an important tool to characterize their multifrequency behaviour. Previous own observations with the VLA at 4.85 GHz, partly published in Nass et al., 1996, and two large ongoing VLA surveys at 1.4 GHz in the northern sky provide radio fluxes for all but one object. One of the VLA surveys is the NVSS (Condon et al., 1996). For this project the VLA is scanning the whole northern sky with $\delta > -40^\circ$ down to 2.5 mJy with a positional accuracy for point sources between $1''$ and $7''.5$. The completion of this project is planned for the end of 1997 — at the time of writing of this paper many areas remain to be observed and processed.

The other survey is the FIRST survey (White et al., 1997) which is performed with higher resolution and sensitivity on selected sky fields. The patchy second HRX area falls nearly totally on the FIRST survey area. For all BL Lac objects in our sample whose position fell within the VLA surveys, a radio counterpart was found. The only object for which we give no radio flux measurement, RX J1451.4+6354, was not covered by own measurements or by either of the two VLA surveys.

For 32 of the 39 objects the two fluxes at 1.4 GHz and 4.85 GHz enabled us to determine the radio spectral index α_R ($f_\nu \propto \nu^{\alpha_R}$) (see Table 2). Variability between the two measurements is possible, and therefore a more reliable determination of the radio spectral index needs dedicated measurements. There is no $\alpha_R < -1$ and most objects show flat $\alpha_R > -0.5$ which is a characteristic property of BL Lac objects (Urry & Padovani, 1995). Possibly some of the steeper α_R (e.g. -0.8 for RX J1422.6+5801) are due to variability between the two measurements.

2.3. X-ray properties

The selection of the objects is based on the ROSAT PSPC countrate between $0.5\,\mathrm{keV} < \mathrm{E} < 2.0\,\mathrm{keV}$ in the RASS. The conversion factor between flux and countrate for a power law with low energy absorption by photoionization depends on the photon index Γ and the hydrogen column density $\mathrm{N_H}$. We assume only Galactic $\mathrm{N_H}$ taken from the Stark et al. (1992) survey and no additional intrinsic absorption. The photon index Γ was calculated individually for each object with the hardness ratios tabulated in the RASS-BSC. The method is described in detail in Schartel et al. (1996).

Γ and $\mathrm{N_H}$ were also determined simultaneously with the two hardness ratios, which yields large uncertainties for low fluxes. We compared the freely fitted $\mathrm{N_H}$ with the Galactic $\mathrm{N_H}$ and found that for all objects the Galactic $\mathrm{N_H}$ lies inside the 2σ errors of the freely fitted $\mathrm{N_H}$.

A common feature of QSO and Seyfert 1 ROSAT spectra is the so-called soft X-ray excess, an additional thermal component of AGN spectra in the extreme soft X-ray and EUV region (Schartel et al., 1996). This feature is not characteristic of BL Lac objects as our analysis and previous studies (Lamer et al., 1996, Padovani & Giommi, 1996) have shown. The spectral behaviour of BL Lac objects in the soft X-ray region is well described by a simple model and the determination of their flux is unambiguous. The conversion factors of the presented objects for the hard ROSAT band differ by only 15% due to the varying Galactic absorption in the surveyed area. For 35 of 39 objects with Galactic $\mathrm{N_H} < 2.5 \cdot 10^{20}\,\mathrm{cm}^{-2}$ the difference is only 7%.

Luminosities are calculated under the assumption of isotropic X-ray emission which need not be correct for BL Lac objects.

2.4. Optical spectra and redshift determination

Most of the BL Lac objects discussed in this paper have been previously identified as such but without a reliable redshift. We took new high signal to noise spectra in order to determine the redshifts of these objects and of additional unpublished BL Lac candidates which fulfill the sample criteria. In March 1997 the focal reducer MOSCA at the Calar Alto 3.5m telescope was used for four nights to take spectra with spectral resolutions of 6 Å ($4150 - 6650$Å) and 12 Å ($4250 - 8400$Å). The 2 min Johnson R aquisition frames were used for photometry and for checking the BL Lac host galaxy. The B magnitude in Table 2 is drawn from this photometry for the newly discovered objects and has an estimated uncertainty of ca. 0.4 mag. B values for already catalogued objects are taken from the literature (Nass et al., 1996). In April 1997 we took additional spectra for two nights at the WHT on La Palma with the ISIS double spectrograph which yielded a spectral resolution of 10Å between 3700 Å and 8900Å. More details can be found in the observation log (Table 3). In the case of RX J1031.3+5053 we analyzed an additional spectrum taken with the old focal reducer at the 3.5m telescope on Calar Alto. For B2 1215+30 and PG1218+304 we got new spectroscopically determined redshifts from Perlman et al., in preparation. The redshift of RX J1111.5+3452 was kindly provided by Schwope and Hasinger, private communication.

The optical data were reduced within the MIDAS package with an optimized Horne algorithm for the extraction of the spectrum which also provides a $1\,\sigma$ noise estimate of each spectrum based on Poisson statistics. A careful flat field correction was performed. Nevertheless fringing patterns remained in the MOSCA spectra above 7000 Å. The ISIS spectra did not have this problem but they suffered from a variable flat field below 5000 Å. In summary both instruments did not provide optimal results but the observations supplemented each other. Since telescope time is scarce we did not in general reobserve objects with known redshifts, but in two cases where we did so we found a redshift different from the published value. There-

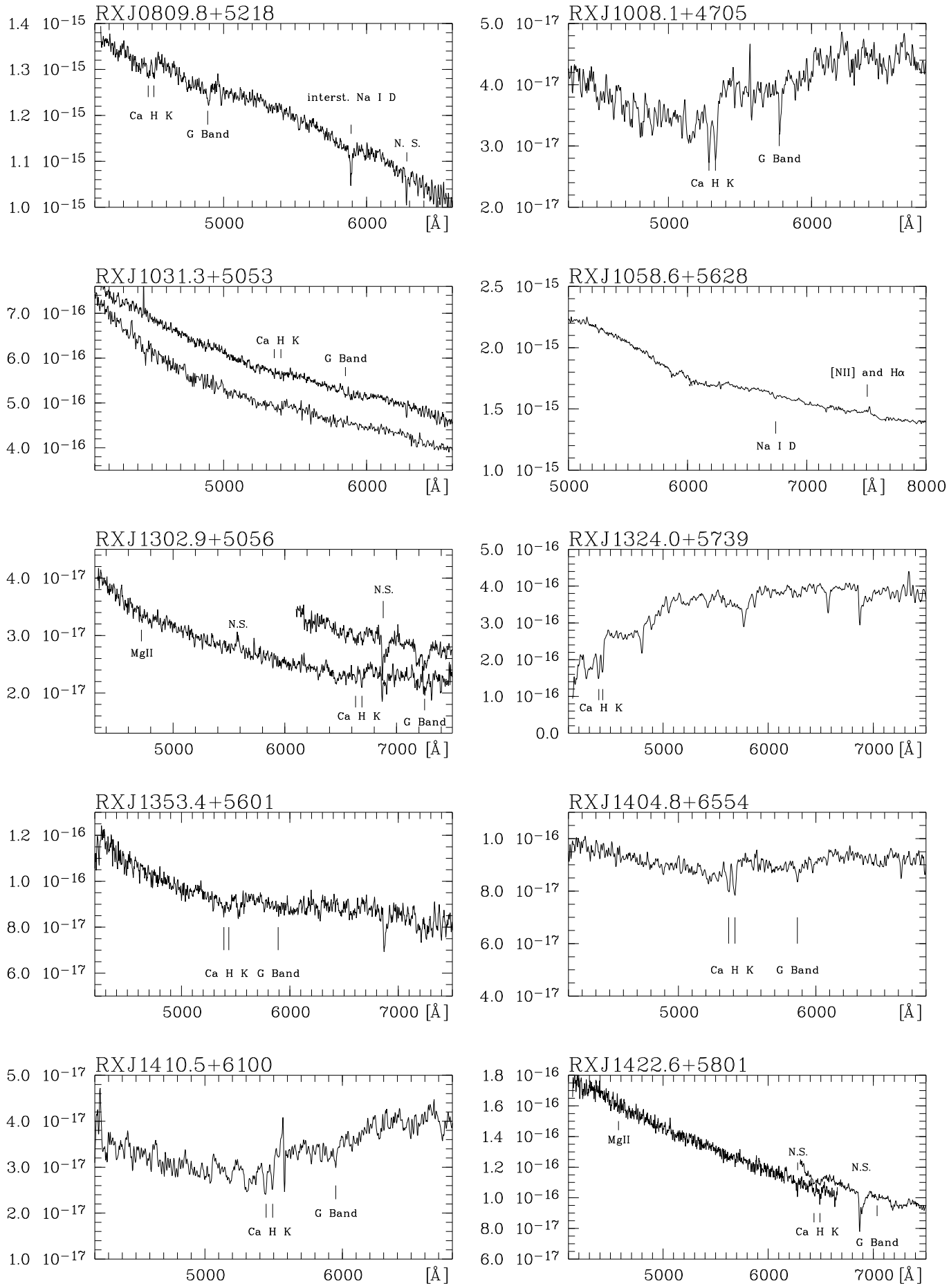
RXJ0809.8+5218
Ca H K
G Band
interst. Na I D
N. S.
RXJ1008.1+4705
Ca H K
G Band
RXJ1031.3+5053
Ca H K
G Band
RXJ1058.6+5628
[NII] and Hα
Na I D
RXJ1302.9+5056
MgII
N.S.
N.S.
Ca H K
G Band
RXJ1324.0+5739
Ca H K
RXJ1353.4+5601
Ca H K G Band
RXJ1404.8+6554
Ca H K
G Band
RXJ1410.5+6100
Ca H K
G Band
RXJ1422.6+5801
MgII
N.S.
N.S.
Ca H K
G Band
[Å]

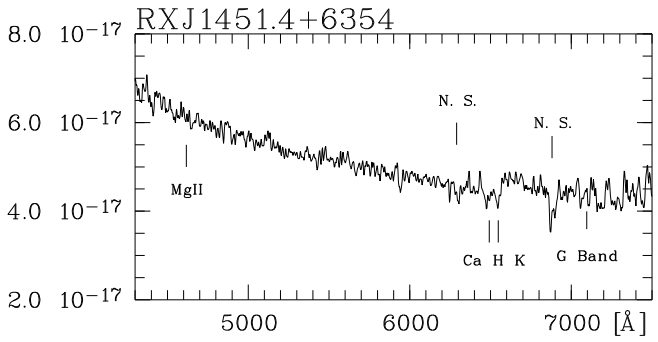
RXJ1451.4+6354
N. S.
N. S.
MgII
Ca H K
G Band
[Å]

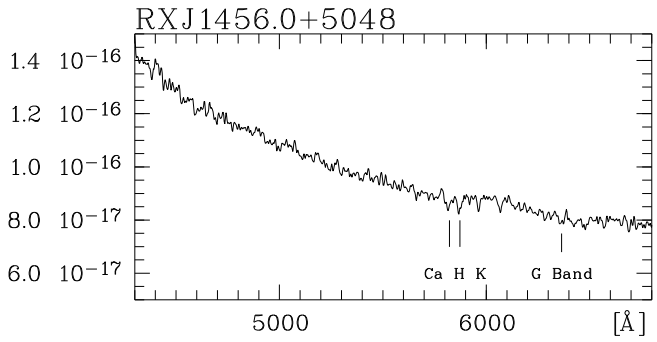
RXJ1456.0+5048
Ca H K
G Band
[Å]

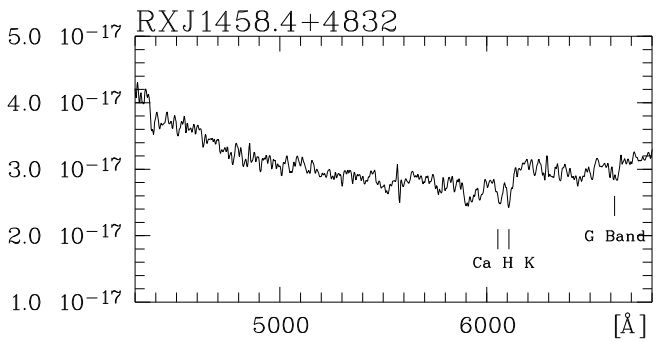
RXJ1458.4+4832
G Band
Ca H K
[Å]

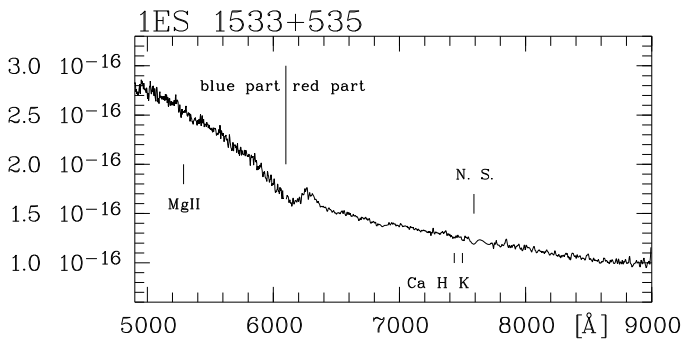
1ES 1533+535
blue part
red part
N. S.
MgII
Ca H K
[Å]

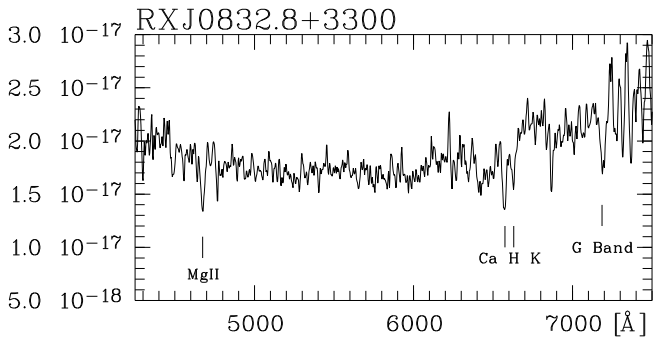
RXJ0832.8+3300
MgII
Ca H K
G Band
[Å]

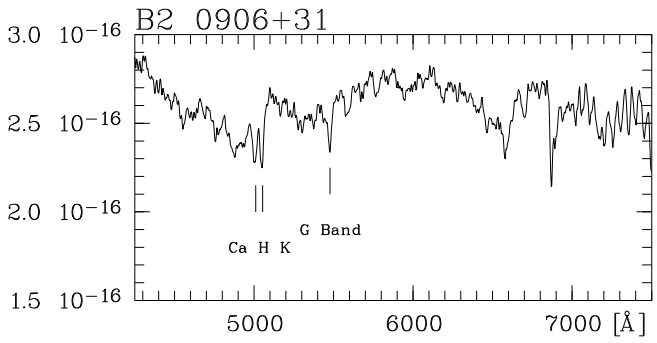
B2 0906+31
Ca H K
G Band
[Å]

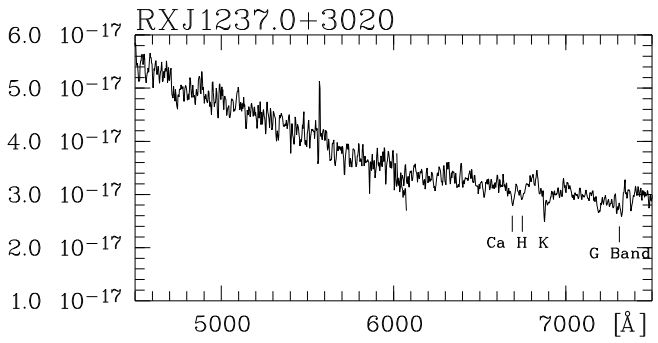
RXJ1237.0+3020
Ca H K
G Band
[Å]

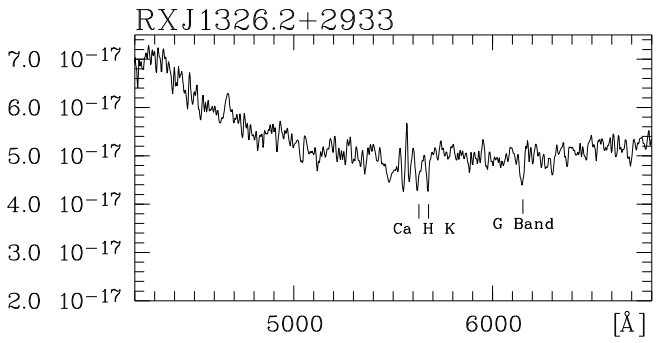
RXJ1326.2+2933
Ca H K
G Band
[Å]

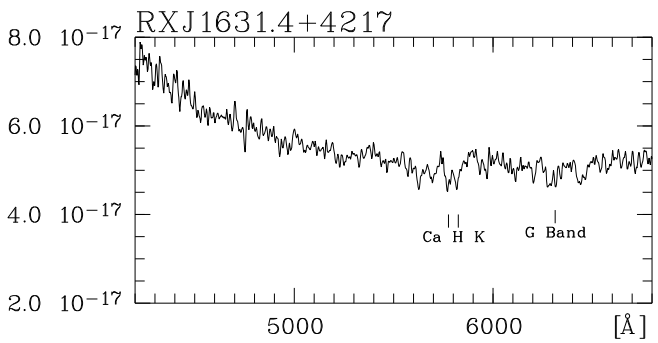
RXJ1631.4+4217
Ca H K
G Band
[Å]

Table 2. BL Lac objects with hard ROSAT countrate above $0.075\,\mathrm{cts\,s^{-1}}$ in the surveyed area. Objects forming the flux limited sample are marked with an asterisk. Positions are measured with an accuracy of $2''$ on the HQS direct plates, or are taken from POSS II in the case of objects too faint to be visible on the HQS plates. Column "cps" lists the countrate $[s^{-1}]$ for the hard ROSAT band ($0.5-2.0\,\mathrm{keV}$), "f_X" is the X-ray flux $[10^{-12}\,\mathrm{ergs\,cm^{-2}\,s^{-1}}]$, "mag" is the optical magnitude B, "f_R" is the radio flux [mJy] from the NVSS at 1.4 Ghz, "Γ" is the photon index ($\mathrm{N(E)} \propto \mathrm{E}^{-\Gamma}$)), "$\log L_X$" is the logarithm of the monochromatic X-ray luminosity $[\mathrm{W\,Hz^{-1}}]$ at 2 keV, "$\log L_R$" is the logarithm of the monochromatic radio luminosity $[\mathrm{W\,Hz^{-1}}]$ at the appropriate frequency, "α_{OX}" is the optical-xray spectral index as defined in footnote 1 and "α_R" is the radio spectral index between 1.4 and 4.85 GHz

Name	R.A. (2000.0)	Decl.	z	cps	f_X	mag	f_R	Γ	$\log L_X$	M_{abs}	$\log L_R$	α_{OX}	α_R
RX J0809.8+5218*	08 09 49.0	52 18 56	0.138	0.371	4.68	15.6	183	2.96	19.54	−24.1	25.0	1.36	−0.3
RX J0916.8+5238*	09 16 52.0	52 38 27	0.190	0.175	2.00	19.7	83	2.18	19.70	−20.7	25.0	0.82	−0.5
RX J0930.6+4950*	09 30 37.6	49 50 24	0.186	1.154	13.45	18.0	22	1.88	20.58	−22.4	24.5	0.74	−0.3
RX J1008.1+4705*	10 08 11.4	47 05 20	0.343	0.383	4.32	18.9	5	2.14	20.63	−22.9	24.6	0.81	−0.1
GB1011+496*	10 15 04.0	49 25 59	0.200	0.594	6.64	16.5	378	2.26	20.26	−24.0	25.7	1.10	−0.4
RX J1031.3+5053*	10 31 18.6	50 53 34	0.361	1.561	17.75	16.8	38	2.31	21.26	−25.1	25.3	0.91	−0.4
RX J1058.6+5628*	10 58 37.8	56 28 09	0.144	0.120	1.33	15.8	229	2.32	19.23	−24.0	25.3	1.45	−0.2
Mrk180*	11 36 26.6	70 09 25	0.046	1.711	19.57	14.7	222	2.26	19.37	−22.5	24.4	1.18	−0.4
RX J1136.5+6737*	11 36 30.3	67 37 05	0.135	0.977	11.40	17.6	46	1.89	20.21	−22.0	24.5	0.82	−0.1
MS 12292+6430*	12 31 31.5	64 14 16	0.164	0.166	1.96	17.4	59	2.02	19.59	−22.7	24.8	1.14	0.0
MS 12354+6315*	12 37 39.1	62 58 41	0.297	0.139	1.64	19.0	13	1.89	20.11	−22.5	24.7	0.92	
RX J1248.3+5820*	12 48 18.5	58 20 27		0.152	1.70	16.3	245	2.42				1.35	−0.1
RX J1302.9+5056*	13 02 55.5	50 56 17	0.688	0.241	2.78	20.2	3	1.94	21.19	−22.9	24.8	0.60	0.8
RX J1324.0+5739*	13 24 00.0	57 39 16	0.115	0.096	1.11	17.3	40	2.04	19.01	−21.5	24.4	1.16	−0.4
RX J1353.4+5601*	13 53 28.0	56 00 55	0.370	0.114	1.31	18.9	15	2.01	19.96	−22.6	24.8	0.91	−0.2
RX J1404.8+6554*	14 04 49.6	65 54 30	0.364	0.091	1.06	19.0	15	2.26	20.06	−22.5	25.0	0.95	
RX J1410.5+6100*	14 10 31.7	61 00 10	0.384	0.116	1.36	20.1	12	1.90	20.28	−21.5	24.4	0.72	−0.8
RX J1422.6+5801*	14 22 39.0	58 01 55	0.638	0.867	9.99	18.7	13	2.06	21.65	−24.1	24.9	0.63	−0.8
RX J1436.9+5639*	14 36 57.8	56 39 25		0.087	1.00	18.8	21	2.22				1.06	−0.5
1E14435+6349 *	14 44 36.6	63 36 26	0.299	0.091	1.07	19.6	19	1.83	19.94	−21.4	24.9	0.82	
RX J1451.4+6354*	14 51 27.5	63 54 19	0.650	0.077	0.89	19.6		2.38	20.59	−23.3		0.91	
RX J1456.0+5048*	14 56 03.7	50 48 25	0.480	0.734	8.58	19.3	4	2.06	21.28	−23.3	24.7	0.64	
RX J1458.4+4832*	14 58 28.0	48 32 40	0.539	0.224	2.68	20.2	3	1.90	20.92	−22.2	24.6	0.61	
RX J1517.7+6525*	15 17 47.6	65 25 21		0.673	8.01	15.5	39	2.06				1.19	−0.6
1ES 1533+535*	15 35 00.8	53 20 35	0.890	0.691	8.01	18.2	18	1.94	21.93	−25.5	25.6	0.72	−0.4
RX J16443+4546*	16 44 19.8	45 46 45	0.220	0.077	0.89	18.7	170	2.36	19.45	−22.1	25.4	1.11	−0.8
IZw187*	17 28 18.4	50 13 10	0.055	1.212	14.59	16.0	168[1]	2.02	19.47	−21.1	24.3	0.95	
RX J0809.6+3455*	08 09 38.5	34 55 37	0.082	0.204	2.63	17.0	224	2.87	18.83	−21.5	24.7	0.89	0.0
RX J0832.8+3300	08 32 52.0	33 00 11	0.671	0.099	1.27	20.7	4	1.57	20.84	−22.3	24.8	0.62	0.0
B2 0906+31*	09 09 53.3	31 06 02	0.274	0.185	2.18	17.8	78[1]	2.21	20.09	−23.0	25.5	1.01	0.2
B2 0912+29*	09 15 52.2	29 33 20		0.286	3.35	16.3	342	2.19				1.15	−0.5
RX J1111.5+3452*	11 11 30.9	34 52 01	0.212	0.233	2.73	19.5	4[1]	2.29	19.92	−21.2	23.8	0.81	−0.3
B2 1215+30*	12 17 52.0	30 07 02	0.130	1.007	11.55	15.6	430	2.46	20.03	−24.0	25.5	1.16	−0.1
PG1218+304*	12 21 21.8	30 10 37	0.182	0.776	9.05	17.7	72	2.09	20.34	−22.6	24.9	0.86	0.0
RX J1230.2+2518	12 30 14.0	25 18 07		0.115	1.33	15.7	351[1]	2.14				1.44	
RX J1237.0+3020*	12 37 05.7	30 20 03	0.700	0.276	3.22	20.0	6	1.85	21.28	−23.1	24.8	0.60	0.0
RX J1241.6+3440	12 41 41.4	34 40 31		0.091	1.06	20.2	10	1.93				0.75	0.1
RX J1326.2+2933	13 26 15.0	29 33 30	0.431	0.128	1.46	19.6	28	2.11	20.39	−22.3	24.8	0.81	−0.8
RX J1631.4+4217*	16 31 24.7	42 17 02	0.468	0.250	2.88	19.5	7	1.91	20.80	−22.6	24.7	0.70	0.0

[1] 4.85 GHz fluxes measured with VLA D configuration

fore it would be strongly desirable to reobserve at least these BL Lac objects for which the redshift is marked in the literature as tentative or ambiguous.

The characterizing feature of optical BL Lac object spectra is a nonthermal featureless continuum which is well described with a single power law. A second component is contributed by the host galaxy. A redshift determination is possible only with this component. The host galaxies are in the majority giant elliptical galaxies (Wurtz et al., 1996). These galaxies have strong absorption features which are produced by the sum of their stellar content. Strong absorption lines in the optical wavelength region of elliptical galaxies and also of most spiral galaxies are an iron feature at 3832 Å, Ca H and K (3934 Å and 3968 Å, respectively), the G Band at 4300 Å, Mg Ib at 5174 Å and the Na I D doublet (5891 Å). Another important feature is

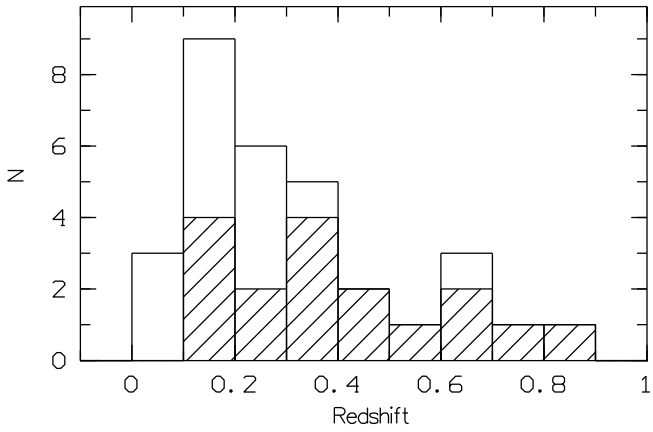

Fig. 2. Redshift distribution of the 31 BL Lac objects from the complete sample. There are 4 more objects in the complete sample without reliably determined redshift. Objects with $\alpha_{\rm OX} < 0.91$ are shaded

the absorption edge at 4000 Å which has a contrast of more than 40% in galaxies with a late stellar population.

The interstellar gas contributes weak narrow emission features to the spectrum. They are weak in normal elliptical galaxies but the most powerful elliptical galaxies, cD galaxies, often show LINER properties and therefore have stronger emission lines.

For a reliable redshift determination we adopted the rule that at least two spectral features must be unambiguously discernible. The strength of the absorption features depends on the flux ratio between the nonthermal featureless continuum and the host galaxy contribution. The strongest absorption line in the optical wavelength region of galaxies is the Ca K line with a typical equivalent width of $\rm W_\lambda = 7$Å (Kennicutt, 1992). In our high signal to noise spectra absorption lines can be detected down to ca. $\rm W_\lambda = 0.3$Å (the spectra of the optical faint objects have lower S/N and thus a higher detection limit for lines). Therefore it becomes impossible to detect Ca K in our spectra if the host galaxy portion is lower than 0.05 or the magnitude difference is larger than 3.5 mag between host galaxy and nonthermal continuum.

For higher redshifts Ca H and K move out of the optical wavelength region, while absorption lines produced by the interstellar gas of the host galaxy become observable. The strength of these lines depends on the relevant ion column density and is in principle independent of the stellar content of the galaxy. It depends on the gas column density, its ionization state, metal composition, and optical depth. These lines are the typical quasar absorption lines. The strongest lines for objects around $\rm z = 1$ are the MgII doublet (2796.4Å and 2803.5Å), MgI 2853.0Å, the two FeII lines (2382.8Å and 2600.2Å), and FeI 2484.0Å, which have equivalent widths up to several Å (Verner et al., 1994). It is difficult to distinguish these lines from ones produced by intervening material. Therefore redshifts derived on this basis are lower limits rather then firm values as derived from lines produced by the stellar population. Moreover, since the gas content of elliptical galaxies is low the expected equivalent widths are small and are possibly at the detection limit of our spectra.

Table 3. Integration times and redshift confidence for the BL Lac objects observed March 1997 with the Calar Alto 3.5m (CA3.5) telescope and April 1997 with the 4.2m telescope (WHT) on La Palma

Name	CA3.5 $[min]$	WHT $[min]$	redshift[1]
RX J0809.8+5218	60		C
RX J1008.1+4705	45		C
RX J1031.3+5053	55[2]		T
RX J1058.6+5628		45	C
RX J1248.3+5820		30	
RX J1302.9+5056	95	60	C
RX J1324.0+5739	25		C
RX J1353.4+5601	30		T
RX J1404.8+6554	30		C
RX J1410.5+6100	40		C
RX J1422.6+5801	85	60	C
RX J1436.9+5639	30	60	
RX J1451.4+6354	30		C
RX J1456.0+5048	70		C
RX J1458.4+4832	60		C
RX J1517.7+6525	30		
1ES 1533+535	60	60	P
RX J0832.8+3300	105		C
B2 0906+31	30		C
RX J0915.8+2933	60		
RX J1230.2+2518		60	
RX J1237.0+3020	120	60	C
RX J1241.6+3440	45	60	
RX J1326.2+2933	30		C
RX J1631.4+4217	56		C

[1] redshift C: certain, T: tentative, P: possible
[2] Includes 25min from March 1994

The ratio between AGN continuum and host galaxy contribution can also be constrained by analyzing the spatial profile of the direct image of the BL Lac object. We have compared the BL Lac images from the 2 min R aquisition frames with star images on the same frame. We found significant deviations from a stellar appearance for all BL Lac objects for which we could determine the redshift including the objects with higher redshift $\rm z > 0.5$. Most of the objects without reliable redshift revealed no extension and could be well described with a stellar appearance. Three of these objects are optically bright, $\rm B < 16.5$. A bright host galaxy with $M_B = -21$ at $\rm z = 0.25$ would appear already 3.5 mag fainter than the nucleus. Therefore we assume $\rm z \geq 0.25$ for these optically brighter objects. Fainter host galaxies would decrease the lower limit for the redshift. The constraints for the optically fainter objects are stronger. We expect $\rm z \geq 0.6$, when the 4000 Å break moves out of the R band.

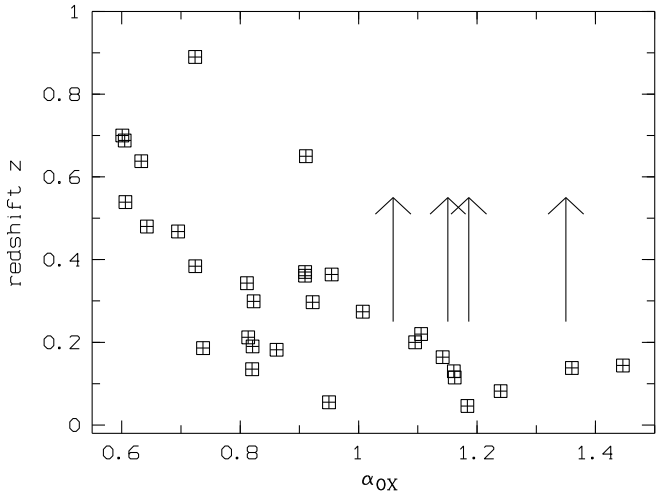

Fig. 3. Redshift versus $\alpha_{\rm OX}$. The objects with unknown redshifts are indicated with arrows

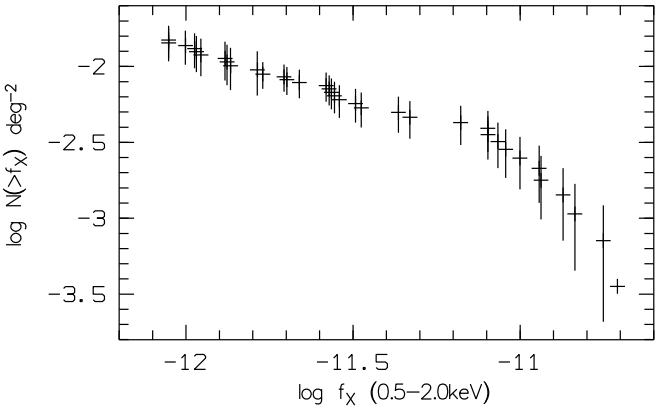

Fig. 4. $\log N(>S) - \log S$ distribution for the complete sample. Only objects above the completeness level have been taken into account

In Fig. 1 the optical spectra are shown. Many spectra were taken under non-photometric conditions. Therefore the spectrophotometric use of the spectra is strongly limited. For some objects we show two spectra taken with different telescopes. In general, they do not join due to different atmospheric conditions and intrinsic variability. The spectra are smoothed with a Gaussian filter of width appropriate to the FWHM of the instrument used. The most important features for the determination of the redshift are marked. We present only objects for which we could determine a new redshift. The other spectra contain no real information and show only a high signal to noise power law with some telluric absorptions. Some of the spectra show severe deviations from a power law, they are produced by a large contribution from the host galaxy. In other spectra features used for the redshift determination have the same strength as telluric and residual flat field features. In such cases the $1\,\sigma$ noise estimate is helpful. The certainty of spectral features significantly increases if they are found in spectra taken with different grisms and telescopes. Comments on individual objects are given in the appendix. They are summarized in Tab. 3.

3. Analysis

3.1. Comparison to existing samples

The $\log N(>S) - \log S$ distribution (Fig. 4) is independent of the subtle redshift determination process for BL Lac objects. Our sample shows a steep slope consistent with the Euclidean value of -1.5 down to $\mathrm{f_X} = 8 \cdot 10^{-12}\,\mathrm{ergs\,cm^{-2}\,s^{-1}}$. Below this flux we have an extremely flat slope of -0.5. The flattening cannot be due to incompleteness since the HRX is fully identified down to the flux limit. If the statistical uncertainties and the different energy ranges[2] are taken into account the distribution is compatible with the surface density we previously published (Nass et al., 1996) which was derived from a larger sky area. However there are deviations to the EMSS sample of BL Lac objects (Maccacaro et al., 1988). The biggest difference arises around our turnover point near $\mathrm{f_X} = 8 \cdot 10^{-12}\,\mathrm{ergs\,cm^{-2}\,s^{-1}}$. This difference could be caused by the fact that the EMSS discarded the targets of the pointed observations which were used to select the serendipitous X-ray sources. Some targets were X-ray bright BL Lac objects. There are further differences between the EMSS and the RASS sample, e.g. the spectral window used for the selection process. In principle, theses differences could be responsible for the small distinctions of $\log N(>S) - \log S$ in both surveys. Near our flux limit the space densities from the two independent surveys are fully consistent. The EMSS found a turnover point in the $\log N(>S) - \log S$ curve around $10^{-12}\,\mathrm{ergs\,cm^{-2}\,s^{-1}}$ (Maccacaro et al., 1988). This cannot be verified with our sample since it is near our flux limit.

Our BL Lac sample is selected from a sky area approximately three times larger than the effective sky area of the EMSS. This presumably explains the fact that we found three objects with $\mathrm{z} < 0.1$ and the EMSS none. The selection process of the EMSS might also have played a role for bright nearby objects. But it is surprising that we found more objects with higher redshifts $\mathrm{z} > 0.4$ and also objects with higher redshifts than present in the EMSS ($\mathrm{z} = 0.638$). The redshift distribution is also flatter but there is still a bump around $\mathrm{z} = 0.2$. This bump in the distribution nearly disappears if only the extremely X-ray dominated BL Lac objects with $\alpha_{\rm OX} < 0.91$ (the median of $\alpha_{\rm OX}$) are taken into account. The low redshift objects are excluded with this criterion and the distribution is more similar to the radio selected BL Lac objects from the 1 Jy sample (Stickel et al., 1991). It is improbable that the objects with unknown redshifts, if included, would destroy this distinction. Most objects with unknown redshift have $\alpha_{OX} > 0.91$ and we have already argued in Sect. 2.4 for medium redshifts $0.25 < \mathrm{z} < 0.7$ for these objects. The bump around $\mathrm{z} = 0.2$ will remain and the objects with unknown redshift cannot be low redshift ob-

[2] assuming a power law with $\Gamma = -2.1$ the abscissa in Fig. 4 values have to be shifted by 0.36 to be comparable with the full ROSAT energy range ($0.1 - 2.4$ keV) or 0.20 for the *Einstein* range ($0.3 - 3.5$ keV), respectively

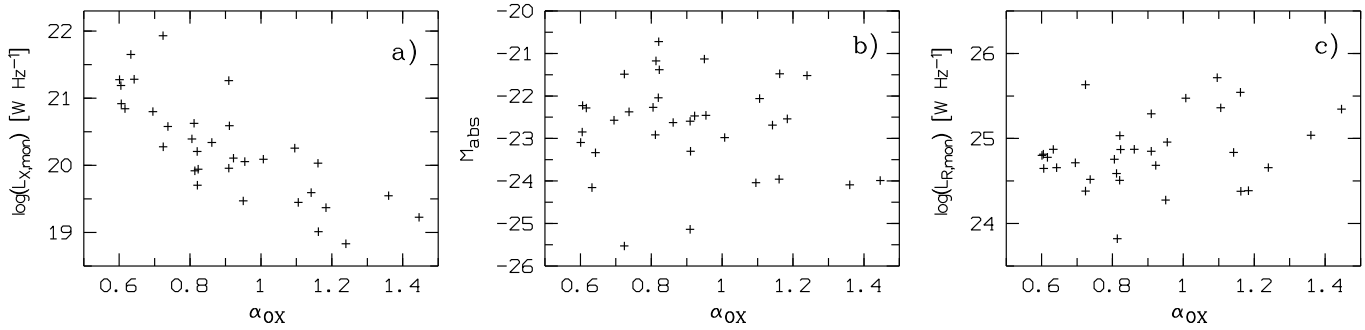

Fig. 5. Luminosities in three wavelength bands versus $\alpha_{\rm OX}$. a) monochromatic X-ray luminosity at 2keV b) absolute optical magnitude c) monochromatic radio luminosity

jects with low $\alpha_{\rm OX}$. We will come back to this important result after the calculation of the luminosity function.

Although the redshift distribution of the extremely X-ray dominated objects is rather flat, somewhat similar to the distribution of the 1 Jy BL Lac sample (Stickel et al., 1991), the analogy cannot be driven too far. The majority of the higher redshifts $\rm z > 0.4$ in the 1 Jy sample were determined with emission lines and the strongest lines often had equivalent widths around the 5Å limit. In our RASS selected sample all redshifts are determined with absorption features and the equivalent widths of the few emission lines which have been detected in some objects (see Appendix) are far below 5 Å. Furthermore some of the emission lines in the 1 Jy sample are resolved and broad ($> 500\,{\rm km\,s^{-1}}$) which is a characteristic feature of Seyfert 1 or QSO activity. All emission lines in our objects are unresolved ($< 500\,{\rm km\,s^{-1}}$) and fully consistent with an origin in HII-regions in the host galaxy — no Seyfert nucleus is necessary to account for these emission lines. The absence of emission lines seems to be a common feature of the optical spectra of X-ray selected BL Lac objects since the spectra of the EMSS objects also show no emission lines (Morris et al., 1991). This distinction between X-ray and radio selected BL Lac objects can be interpreted as an indication of differing parent populations in X-ray and radio selected BL Lac objects.

3.2. Luminosity function

Redshifts are available for 31 (89%) of the 35 BL Lac objects forming a flux limited sample. This high portion of objects with known redshifts allows the determination of a luminosity function. Possible biases and selection effects introduced by the objects with unknown redshifts, which have been excluded from the luminosity function, are discussed later.

Determination of a luminosity function means taking all objects above the flux limit, counting the objects above a given luminosity, and dividing the number by the volume surveyed for these objects. The BL Lac sample is distributed on two subareas with different flux limits which do not overlap (see Sect. 2.1). The results of each area are combined with the methods given in Avni & Bahcall (1980).

A first step to evaluate the contribution of each object to the luminosity function is the calculation of the maximal redshift $\rm z_{max}$ where this object would be detectable with the given flux limit. For this purpose a K-correction is assumed which depends on the individually determined power law spectra. It should be noted that it is not clear that the power law can be extrapolated as far as it would be needed by the largest $\rm z_{max}$ which are around $\rm z = 2$.

Finally a luminosity function is obtained with this procedure which is determined between the minimal and maximal redshift of the sample, but which assumes no evolution. However, the objects are not evenly distributed in the volume, $\langle V/V_{max}\rangle$ being 0.40 ± 0.06 rather than 0.5 as expected for a uniform distribution. It is common practice to determine luminosity functions under the assumption of $\langle V/V_{max}\rangle = 0.5$ and a redshift dependent cosmological evolution. We have investigated density evolution with the parameterization $\rho(\rm z) = \rho(0)\cdot(1+z)^{\beta}$ and luminosity evolution in the form $L_X(\rm z) = L_X(0)\cdot(1+z)^{\gamma}$. $\langle V/V_{max}\rangle = 0.5$ is achieved for $\beta = -4.0$ with $\pm 2\sigma$ limits of -7.6 and $+0.2$ and for luminosity evolution we obtain $\gamma = -4.9$ with $\pm 2\sigma$ limits of -13.6 and 0.2 (see also Table 4). If 1ES 1533+535 is omitted from the analysis, the object with the highest but also most uncertain redshift, the evolution parameters α and γ are slightly shifted to stronger negative evolution. We now consider how this result might be affected by the objects with unknown redshift. In Sect. 2.4 we have already argued that these objects have a high probability of high redshift. For a check we have adopted $\rm z = 0.3$ and $\rm z = 0.7$ for these objects and repeated the analysis. The changes for the evolution parameters are small. In both cases the $\pm 2\sigma$ limits are decreased because the statistics are better, but otherwise there is little change. These results can be generalized, if some of our tentative redshifts are not correct. In such a case the evolution parameters will only slightly be altered. However, the form of the luminosity function could be changed. In particular, if our sample consists several objects with $\rm z > 1$ the luminosity function will be enlarged to higher luminosities.

In principle, our analysis of the luminosity function of RASS selected BL Lac objects has given similar results compared to the analyses performed with EMSS selected objects (Morris et al., 1991 and Wolter et al., 1994). Our sample shows

Table 4. Cosmological evolution parameters and $\langle V/V_{max}\rangle$ for the complete sample

	N	β	β, 2σ range	γ	γ, 2σ range	$\langle V/V_{max}\rangle$
unknown redshifts omitted	31	-4.0	$-7.6 < \beta < +0.2$	-4.9	$-13.6 < \gamma < +0.2$	0.40 ± 0.06
without 1ES 1533+535	30	-4.0	$-8.1 < \beta < +0.7$	-4.6	$-13.8 < \gamma < +0.5$	0.41 ± 0.06
unknown redshifts set to $z = 0.3$	35	-3.7	$-7.2 < \beta < +0.3$	-4.3	$-12.0 < \gamma < +0.2$	0.41 ± 0.05
unknown redshifts set to $z = 0.3$, $\alpha_{\rm OX} > 0.91$	18					0.48 ± 0.08
unknown redshifts set to $z = 0.3$, $\alpha_{\rm OX} < 0.91$	17					0.34 ± 0.06
unknown redshifts set to $z = 0.7$	35	-3.2	$-6.4 < \beta < +0.6$	-3.7	$-10.9 < \gamma < +0.5$	0.42 ± 0.05
unknown redshifts set to $z = 0.7$, $\alpha_{\rm OX} > 0.91$	18					0.49 ± 0.08
unknown redshifts set to $z = 0.7$, $\alpha_{\rm OX} < 0.91$	17					0.34 ± 0.06

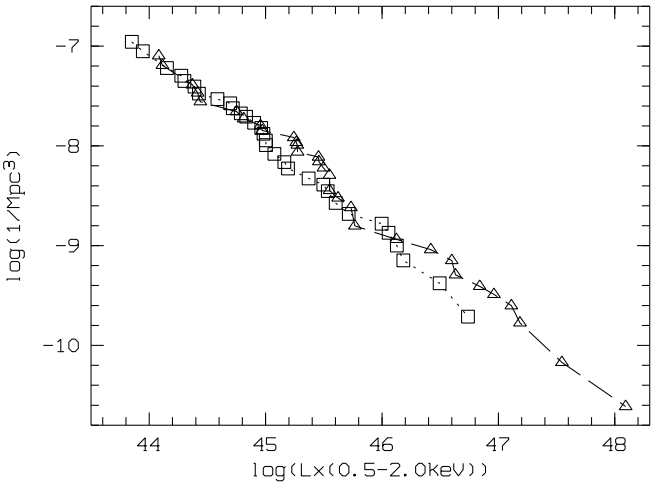

Fig. 6. Cumulative luminosity function for RASS selected BL Lac objects evolved to $z = 0$ with the assumption of density evolution (marked with squares) and luminosity evolution (triangles). Objects with unknown redshifts are not considered

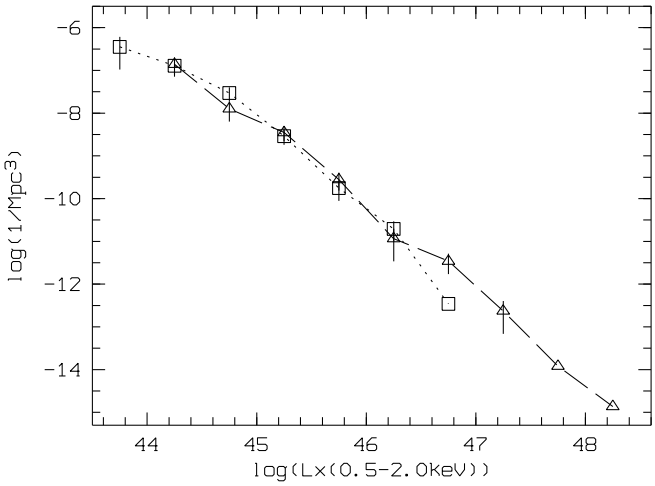

Fig. 7. Differential luminosity function for RASS selected BL Lac objects evolved to $z = 0$, same coding as in Fig. 6. The bin size of the x-axis is 0.5, the y-axis gives the space density per luminosity interval of $10^{44}\,\mathrm{ergs\,s^{-1}}$

negative evolution, too, although in a milder form. The complete RASS sample contains 13 more objects than the sample presented in Morris et al. (1991) and 3 more than in Wolter et al. (1994). Therefore the statistics are a little better, nevertheless negative evolution is not ruled out on the 2σ level if we adopt $z = 0.3$ or $z = 0.7$ for the objects with unknown redshift. Because most of these objects are optically bright, redshifts closer to $z = 0.3$ are probable. A detailed comparison of the cumulative luminosity function, shown in Fig. 6, with previously published functions is limited by the different evolution parameters which alters the space densities. We cannot find strong deviations, the most important difference is the extension of the RASS luminosity function to higher luminosities by at least one order of magnitude. The differential luminosity function, shown in Fig. 7, can be well described by a single power law with no significant bump and with a flat index -1.9. The statistics are too low for building redshift bins, so this cannot be used to distinguish between density and luminosity evolution. Because luminosity evolution foresees extremely powerful BL Lac objects at $z = 0$ which are not observed, we favour density evolution.

3.3. Evolutionary behaviour and spectral energy distribution

The V/V_{max} variable, first introduced by Schmidt (1968), can itself be used to discuss the cosmological evolution of objects. V/V_{max} depends mainly on the ratio between observed flux and the survey flux limit, with a weaker dependence on the observed redshift and cosmological model.

Motivated by the contradicting results about the evolutionary behaviour in X-ray and radio selected BL Lac objects we divided our sample into two subsamples according to the X-ray dominance in the spectral energy distribution. The extremely X-ray dominated objects with $\alpha_{\rm OX} < 0.91$ have $\langle V/V_{max}\rangle = 0.34 \pm 0.06$ and the intermediate objects have $\langle V/V_{max}\rangle = 0.48 \pm 0.08$. With a Kolmogorov-Smirnov test we obtain a probability of 0.19 for the null hypothesis that both subgroups are taken from the same parent sample. The $\langle V/V_{max}\rangle$ statistic develops with $1/\sqrt{12N}$. Again the effect of objects with unknown redshift must be checked. They are unevenly distributed in this case (see Fig. 3). All these objects have $\alpha_{\rm OX} > 0.91$ with one object having exactly the median value. The changes introduced by the 4 objects are small if we adopt $z = 0.3$ or $z = 0.7$ for them (see Table 4). Statistically

the difference of $\langle V/V_{max}\rangle$ is only significant at the 2σ level. This result matches well with previously published analyses, leading us to believe in the reality of this observation. Apparently contradictory results relating to cosmological evolution in X-ray selected (Morris et al., 1991) and radio selected (Stickel et al., 1991) BL Lacs are resolved in our sample. The bump around $\mathrm{f_X} = 8 \cdot 10^{-12}\,\mathrm{ergs\,cm^{-2}\,s^{-1}}$ in the $\log \mathrm{N}(>\mathrm{S}) - \log \mathrm{S}$ distribution (Fig. 4) is also mainly produced by the objects with low α_{OX}. In a $\log N(>S) - \log S$ plot with only these objects the bump is exaggerated whereas for objects with $\alpha_{\mathrm{OX}} > 0.91$ it is insignificant (but does not totally disappear).

In Sect. 3.1 we found a distinction in the redshift distribution for the two BL Lac object subgroups in Sect. 3.1. Here the statistical significance is higher, a Kolmogorov-Smirnov test yields a probability of 0.009 for the null hypothesis. Even if $\mathrm{z} = 0.7$ is adopted for the unknown redshifts the distinction between the two subgroups remains. All objects with $\mathrm{z} < 0.1$ have $\alpha_{\mathrm{OX}} > 0.91$. Figure 3 implies an anticorrelation between α_{OX} and z, but the significance of this relation is reduced by the unknown redshifts. As for luminosities, both the uneven redshift and the V/V_{max} distribution have similar effects, so that it can be stated that the X-ray luminosity distributions of X-ray dominated and intermediate objects are clearly distinct, with a probability of 0.002 for a common parent population.

In order to look for additional confidence in the redshift distribution distinction we verified other X-ray selected BL Lac samples. If the EMSS BL Lac sample is divided into equal halves according to the ratio between X-ray and radio flux, the more X-ray dominated subgroup has higher redshifts, too. The *Einstein* Slew Survey sample (Perlman et al., 1996) is not well suited for such a comparison since the redshift is missing for many of the X-ray dominated objects. But again, no $\mathrm{z} < 0.1$ object is found among the objects with $\alpha_{\mathrm{OX}} < 0.91$, although there are several such objects among the intermediate objects.

3.4. Selection effects

A selection effect described by Browne & Marchã (1993) is that low luminosity and nearby BL Lac objects are difficult to distinguish from their host galaxies because their nucleus is dominated by starlight and does not fulfill the spectroscopic requirements for a featureless optical spectrum. This selection bias cannot be responsible for the higher redshifts in objects with low α_{OX}. Bright objects with small redshifts are also missing in this subgroup. And there is no reason why we should have misidentified all low redshift objects with low α_{OX}, but did select such objects with high α_{OX}.

In X-ray surveys faint BL Lac objects can also be lost in the extended X-ray emission of a rich hosting galaxy cluster. This is only possible if the BL Lac object is considerably fainter in X-rays compared to the surrounding cluster. Therefore only the X-ray faint BL Lac objects can be overpowered by clusters since X-ray clusters reach only X-ray luminosities of several $10^{45}\,\mathrm{ergs\,s^{-1}}$ (Schindler et al., 1996). Therefore consequences of this selection effect are comparable to the problems caused by strong host galaxies. Again, the distinction between objects with low and high α_{OX} is not readily explicable by means of this effect.

4. Discussion

We have determined the luminosity function of RASS selected BL Lac objects which has a larger luminosity range than previously published luminosity functions. The analysis of the evolutionary behaviour confirmed earlier statements about a negative evolution of X-ray selected BL Lac objects. In our sample the negative cosmological evolutionary behaviour is restricted to the extremely X-ray dominated objects with $\alpha_{\mathrm{OX}} < 0.91$. Further hints for two distinct populations can be found in the $\log \mathrm{N}(>\mathrm{S}) - \log \mathrm{S}$ distribution. The bump around $\mathrm{f_X} = 8 \cdot 10^{-12}\,\mathrm{ergs\,cm^{-2}\,s^{-1}}$ is mainly caused by the extremely X-ray dominated objects. In our sample the BL Lac objects with low α_{OX} are a high X-ray luminosity population with few low luminosity objects. There is no clear distinction in optical and radio luminosity between the two subgroups. This is not compatible with the assumption that X-ray selected BL Lac objects are the low luminosity part of a single BL Lac population (Urry & Padovani, 1995). Still, the radio luminosity of most RBLs of the 1 Jy sample exceeds the luminosities found in our sample.

The characteristic features of BL Lac objects are often explained with a relativistic jet aligned to our direction. While this view is widely accepted, more detailed specifications about the physical nature of the jet and the parent population, the objects with jets not pointed towards our direction, are still in debate. Here we want to mention some consequences of our new results on existing models, in particular the different redshift distributions of objects with low and high α_{OX}.

4.1. Unified schemes and the parent population

The unified scheme for BL Lac objects tries to identify X-ray and radio selected BL Lac objects with intrinsically identical parent populations in which only some physical parameters of the jet vary (e.g. beaming properties, angle Θ_C between line of sight and jet). If only one parent population is responsible for BL Lac objects the luminosity function of BL Lac objects has to be consistent with the luminosity function of the parent population under the assumption of physically reasonable beaming properties. Padovani & Urry (1990) investigated whether Fanaroff-Riley type I (FR I) radio galaxies can be a plausible parent population. Assuming a simple beaming model for jets in FR I galaxies described in Urry & Shafer (1984) they calculated the luminosity function of X-ray selected BL Lac objects. In principle they predicted a beamed luminosity function that has a double power law with the same power law index as the parent population above a certain break point and a considerably flatter slope below this point. The predicted break point lies at ca. $\mathrm{L_X} = 10^{43}\,\mathrm{ergs\,s^{-1}}$ and is outside the covered range of our luminosity function.

The power law index (-1.9) of our differential luminosity function is only slightly flatter than the index of FR I galaxies as determined by Padovani & Urry (1990) (-2.1). Given

the uncertainty in the luminosity function of the BL Lac objects and the (similar) uncertainty in that of the FR I galaxies, this difference is not significant. Since negative evolution of BL Lac objects was not in popular discussion, Padovani & Urry (1990) discuss only the effects of positive evolution. To adjust their model for the extremely high X-ray luminosities found in our sample (roughly one order of magnitude higher than in the calculation of their paper) stronger beaming must be assumed with bulk Lorentz factors $\gamma > 7$ which is comparable to values found in radio selected BL Lac objects.

The assumption of one parent population for BL Lac objects is not commonly accepted. Wall & Jackson (1997) allowed radio galaxies of Fanaroff-Riley type I and II to generate BL Lac objects if their jets are aligned towards us. With this scheme they could reproduce 5 GHz source counts of different extragalactic radio source classes, but they had to adopt higher Lorentz factors than determined by Padovani & Urry (1990). The method of Wall & Jackson (1997) cannot be easily transformed to our dataset because the radio data of our X-ray selected sample are inhomogeneous. More detailed radio observations are necessary to investigate whether the differing sample properties of BL Lac objects below and above $\alpha_{OX} = 0.91$ can be attributed to different parent populations.

4.2. Jet models and selection effects

Studies of BL Lac objects have shown that X-ray surveys are an efficient tool to find BL Lac objects, and that X-ray selected BL Lac objects outnumber radio selected objects. This is just what would be expected if X-ray selected objects are intermediate in orientation between radio selected BL Lac objects and radio galaxies. A physically justified explanation for this is an accelerating jet model where the X-rays arise from regions closer to the core than the regions emitting the radio emission. Applying this "wide jet" model, Ghisellini et al., 1993, estimate that radio selected BL Lac objects have an opening angle $\Theta < 15^\circ$ (for which the observer would see comparable radio emission), that X-ray selected objects have $15^\circ < \Theta < 30^\circ$ and that objects with $\Theta > 30^\circ$ appear to the observer as normal radio galaxies. Celotti et al., 1993, used this picture to calculate the luminosity functions of X-ray and radio selected BL Lac objects and in principle they were able to reproduce the observed data. However, this model has problems explaining our result of a redshift distribution dependence on the multifrequency spectrum. The most common objects are the intermediate objects, the extreme X-ray and radio dominated objects have lower space density. Perhaps the model can be adjusted to the correlation between $\alpha_{\rm OX}$ and redshift, but then additional free parameters are needed.

As an alternative to the "wide jet" model Giommi & Padovani (1994) have suggested that the distinction between X-ray and radio selected BL Lac objects is caused by the location of the high energy cutoff of the synchrotron emission and that the two populations are fundamentally the same. In this scenario, X-ray selected BL Lac objects are intrinsically rarer, contrary to the standard view. The larger X-ray numbers originate solely from selection effects. With this scheme the authors can reproduce the redshift and luminosity distribution in the X-ray and radio band for X-ray and radio selected BL Lac samples. However, this interesting scheme does not explain why low redshift objects are not found among the extremely X-ray dominated objects. In our flux limited sample the intermediate objects have the lowest X-ray luminosity. Regarding the optical and radio luminosity there is no clear division into two subgroups.

4.3. Variability in the spectral energy distribution

Multiwavelength observations of outbursts of BL Lac objects could be helpful for understanding the anticorrelation between redshift and $\alpha_{\rm OX}$. Coordinated observations from the optical to the extreme γ-region (TeV-region) of the X-ray bright BL Lac objects Mrk 421 (Macomb et al., 1995) and Mrk 501 (Catanese et al., 1997) revealed strong correlated flux variations in the X-ray and TeV region whereas the correlated variability in the optical region was only small. In March 1997 Mrk 501 varied by a factor of 4 in flux between $2 - 10$ keV and less than 20% in the U-band. During the outburst of Mrk 501 the peak of νf_ν in the X-rays, which is interpreted as the high synchrotron energy cutoff, was located at energies of ~ 100 keV. Catanese et al., 1997 conclude from these observational results that the maximum electron Lorentz factor of Mrk 501 is of the order $\gamma_{\rm max} \sim 10^6$. Macomb et al., 1995, propose that a similar outburst in Mrk 421 could be caused by a change in the upper energy cutoff in the relativistic electron distribution without affecting either the magnetic field or the normalization of the electron energy distribution.

The interesting aspect of these observations is that Mrk 501 and Mrk 421 are objects with $\alpha_{\rm OX}$ typical for intermediate objects, while in times of high activity their $\alpha_{\rm OX}$ decreases to values characteristic for the extremely X-ray dominated objects in our sample. Buckley et al., 1996, suggest that extremely X-ray dominated BL Lac objects also have high synchrotron energy cutoffs. Furthermore we suggest that the extremely X-ray dominated objects with $\alpha_{\rm OX} < 0.91$ are observed in a state of enhanced activity whereas the intermediate BL Lac objects have lower energy cutoffs and they would represent the quiescent population. Because the X-ray luminosities and redshifts of the objects are higher in the 1 Jy survey than for intermediate BL Lac objects this speculative image is not consistent with the idea of a single BL Lac population. However, it offers a simple explanation for the anticorrelation between the redshift and X-ray luminosity and $\alpha_{\rm OX}$.

Kollgaard et al., (1996) measured with radio methods the bulk Lorentz factor γ for several BL Lac objects. They conclude that X-ray selected BL Lac objects have smaller values of γ than radio selected BL Lac objects which is in contradiction to our results in Sect. 4.1 and of Catanese et al., 1997. We note that we would classify almost all X-ray selected objects used for these radio measurements as intermediate, which would solve this discrepancy.

5. Summary and Conclusions

We have shown that the unified models do not predict the distinction between the two subgroups in our sample and additional free parameters would be necessary to adjust the model with the observations. Currently the observational constraints are of low statistical significance. Two populations of BL Lac objects with different physical origin are also consistent with the results. The dividing point, $\alpha_{\rm OX} = 0.91$, is the median of the sample and has no special physical significance.

Our study has confirmed the negative evolution of X-ray selected BL Lac objects and we find that this behaviour could be restricted to the extremely X-ray dominated BL Lac objects. The cosmological evolutionary behaviour of the intermediate objects is consistent with no evolution. Since these two subgroups show a different redshift distribution the interesting evolution time of X-ray dominated BL Lac objects is shifted outside to $1.0 < {\rm z} < 2.0$ (the $\rm z_{max}$ from the V/V_{max} analysis). There is still no answer for this odd behaviour, which up to now has not been found in other AGN classes. Possibly the jets in these objects, which are especially powerful in the X-rays, need a minimal time for development. This speculation has gained some plausibility since the analysis of our sample has shown that the relevant times lie farther away. Nevertheless X-ray dominated BL Lac objects must have been considerably rarer between $2 < {\rm z} < 3$, the time when QSO activity was at its highest point. The distinct properties in the two subgroups are already revealed in the bright part of the $\log N(> S) - \log S$ distribution. It is therefore implausible that selection effects, as described by Browne & Marchã (1993), are responsible for this distinction. Nevertheless, BL Lac objects are "susceptible" to selection effects and therefore, in future, galaxy clusters should be carefully analyzed in the selection process.

The observations suggest the intermediate BL Lac objects as the basic population. They have the lowest luminosity in X-rays and radio wavelengths, and they have the highest space density. Both the extremely radio and X-ray dominated BL Lac objects have higher luminosities. This led us to speculate about a beaming scenario. The spectral energy distribution of extremely X-ray dominated BL Lac objects can be interpreted with a high energy cutoff of the synchrotron spectrum. The high X-ray luminosity of objects with $\alpha_{\rm OX} < 0.91$ can be explained with large bulk Lorentz factor of relativistic electrons in the jets of these objects. This result is compatible with conclusions from multiwavelength observations of outbursts in Mrk 421 and Mrk 501. Therefore we suggest that extreme X-ray dominated objects are observed in a state of enhanced activity which would explain the anticorrelation between X-ray luminosity and $\alpha_{\rm OX}$.

Our investigation has shown the importance of the redshift parameter for the study of samples of BL Lac objects. Advances in observing techniques have made easier the determination of redshifts in optical spectra which are devoid of strong features. In order to have stronger observational constraints it is necessary to enlarge the sample and to determine redshifts for objects for which this has not yet been possible. The uncertainty of the V/V_{max} statistics depends on $1/\sqrt{12N}$. In the last years several projects began to select BL Lac objects with combined X-ray - radio methods (e.g. Wolter et al., 1997). They will certainly yield valuable results about intermediate objects and low flux BL Lac objects below the adopted flux limit in this paper. However, the extremely X-ray dominated BL Lac objects are rare and their negative evolution leads to a very flat $\log N - \log S$. Their distinct population properties are an important tool to understand the BL Lac phenomenon, and they can be selected most preferably with the full sky coverage of the RASS.

Acknowledgements. The ROSAT project is supported by the Ministerium für Bildung, Wissenschaft, Forschung und Technologie (BMBF/DARA) and by the Max-Planck-Gesellschaft (MPG). We thank K. Molthagen for assistance during observations. L. Wisotzki is thanked for providing his implementation of the Horne algorithm. NB acknowledges support by the BMBF under DARA 50 0R 96016.

References

Avni Y., Bahcall J. N., 1980, ApJ 235, 694
Bade N., Engels D., Voges W., et al., 1998, A&AS 127, 145
Blandford, R., Rees M. J., 1978, in Pittsburgh Conference on BL Lac objects, ed. A. M. Wolfe
Browne I. W. A., Marchã M. J. M., 1993, MNRAS 261, 795
Buckley J. H., Akerlof C. W., Biller S., et al., 1996, ApJ 472, L9
Catanese M., Bradbury S. M., Breslin A. C., et al., 1997, ApJ 487, L143
Celotti A., Maraschi L., Ghisellini G., Caccianiga A., Maccacaro T., 1993, ApJ 416, 118
Condon J. J., Cotton W. D., Greisen E. W., et al., 1996, ADIL..JC..01
Cordis L., Bade N., Engels D., Voges W., 1996, MPE-Report 263, 441
Ghisellini G., Padovani P., Celotti P., Maraschi L., 1993, ApJ 407, 65
Giommi P., Padovani P., 1994, MNRAS 268, L51
Jannuzi B. T., Smith P. S., Elston R., 1994, ApJ 428, 130
Hagen H.-J., Groote D., Engels D., Reimers D., 1995, A&AS 111, 195
Kennicutt Jr. R. C., 1992, ApJS 79, 255
Kollgaard R. I., 1994, Vistas in Astronomy, Vol. 38, 29
Kollgaard R. I., Palma C., Laurent-Muehleisen S. A., Feigelson E. D., 1996, ApJ 465, 115
Lamer G., Brunner H., Staubert R., 1996, A&A 311, 384
Laurent-Muehleisen, S. A., 1996, Ph.D. thesis, Pennsylvania State University
Maccacaro T., Gioia I. M., Schild R. E., et al., 1988, Lecture Notes in Physics 334, BL Lac objects, Proceedings, Como, Italy, Springer Verlag, p. 222
Macomb D. J., Akerlof C. W., Aller H. D., et al., 1995, ApJ 449, L99
Marchã M. J. M., Browne I. W. A., Impey C. D., Smith P. S., 1996, MNRAS 281, 425
Morris S. L., Stocke J. T., Gioa I., et al., 1991, ApJ 380, 49
Nass P., Bade N., Kollgaard R. I., et al., 1996, A&A 309, 419
Ostriker J. P., Vietri M., Nature 318, 446
Padovani P., Giommi P., 1996, MNRAS 279, 526
Padovani P., Urry C. M., 1990, ApJ 356, 75
Perlman E., Stocke J. T., Schachter J. F., et al., 1996, ApJS 104, 251
Schartel N., Walter R., Fink H. H., Trümper J., 1996, A&A 307, 33
Schindler S., Hattori M., Neumann D. M., Böhringer H., 1996, A&A 317, 646
Schmidt M., 1968, ApJ 151, 393

Stark A. A., et al., 1992, ApJS 78, 77
Stickel M., Padovani P., Urry C. M., Fried J. W., Kühr H., 1991, ApJ 374, 431
Stocke J. T., Morris S. L., Gioa I., et al., 1990, ApJ 348, 141
Stocke J. T., Morris S. L., Gioa I., et al., 1991, ApJS 76, 813
Urry C. M., Padovani P., 1995, PASP 107, 803
Urry C. M., Shafer R. A., 1984, ApJ 280, 569
Verner D. A., Barthel P. D., Tytler D., 1994, A&AS 108, 287
Voges W., Aschenbach B., Boller Th., et al., 1996, IAU Circ. 6420
Wall J. V., Jackson C. A., 1997, MNRAS 290, L17
White R. L., Becker R. H., Helfand D. J., Gregg M. D., 1997, ApJ 475, 479
Wolter A., Caccianiga A., Della Ceca R., Maccacaro T., 1994, ApJ 433, 29
Wolter A., Ciliegi P., Della Ceca R., et al., 1997, MNRAS 284, 225
Wurtz R., Stocke J. T., Yee H. K. C., 1996, ApJS 103, 109

Appendix

The appendix gives comments on the classification of some objects as BL Lacs if the objects are optically extremely faint or other peculiarities exist. For objects with subtle optical spectral features details of the redshift determination are provided and tentative or ambiguous redshifts are marked.

RX J0809.8+5218 This object has an extremely strong interstellar Na I D absorption line, stronger than the absorption features from the host galaxy. There exists a second optical spectrum with higher resolution which confirms our redshift. This object is also a member of the *Einstein* Slew Survey.

RX J1031.3+5053 In March 1997 a 30min exposure with 6Å spectral resolution was taken. Two weak lines ($W_\lambda = 0.4$Å) were found with the correct separation for Ca H and K. There is a suggestion of the G band in this spectrum but it is barely discernible from the noise. The Ca H and K lines are confirmed in a spectrum with a lower resolution (15Å) spectrum from March 1994, in addition a weak 4000Å break is apparent. This object is also a member of the *Einstein* Slew Survey. We did not find the absorption features indicated by Perlman et al. (1996) in our spectrum which led to a different redshift. This contradiction and the weakness of the absorption feature let us consider the redshift of $z = 0.361$ as tentative although two spectra exist which supplement each other with our redshift.

RX J1058.6+5628 In the red part of the WHT spectrum Na I D absorption is found at 6740Å. It appears broad in accordance with its doublet character. In addition weak emission lines from [NII]6548, Hα and [NII]6584 can be found for this redshift. The strongest emission line, [NII]6584, has an equivalent width of $W_\lambda = 0.9$Å, well below the classification limit. Ca H and K and the G band are strongly affected by varying flatfield corrections in the blue part of our WHT spectra, but they can be found at the appropriate place in spectra taken by Laurent-Muehleisen (1996). We consider this redshift therefore as secure. We cannot confirm the redshift given in Marchã et al. (1996) which is based on [OIII] emission lines at 7000Å where neither our spectrum nor spectra taken by Laurent-Muehleisen (1996) show emission lines.

RX J1302.9+5056 This optically faint object is not visible on the digitized POSS I data and the HQS direct plates. The position is taken from the digitized POSS II data. The spectral features (MgII 2798, Ca H and K and G band) used for the redshift determination have been found on spectra taken with different telescopes.

RX J1324.0+5739 This low luminosity object has very strong absorption features. The contrast of the 4000Å break is, at 24%, at the border of the classification limit. The available radio and X-ray properties are consistent with a BL Lac classification and we adopted it for our analysis. We note that spectra taken by Laurent-Muehleisen (1996) have a stronger 4000Å break and she classified this object as a galaxy. Variability and the exact position and width of the slit can be responsible for this deviation.

RX J1353.4+5600 Ca H and K and the G band are marked in Fig. 1 and a 4000Å break is apparent. These features lead to $z = 0.370$. The comparatively strong absorption feature at 5530Å cannot be explained with this redshift. Since we have taken only one spectrum the redshift has a tentative character.

RX J1422.6+5801 Two absorption lines with the right separation to be Ca H and K are found in spectra with varying resolutions taken at two different telescopes. An absorption line at the redshifted position of MgII 2798 is indicated on the Calar Alto 3.5m spectra and the G band is clearly visible on the WHT red spectrum. The high redshift of $z = 0.638$ together with the high X-ray flux makes this object the most X-ray powerful BL Lac object known up to now.

RX J1456.0+5048 The radio image of this faint object is somewhat confusing. The NVSS lists a radio source with 4.4 mJy 12″ distant from the optical position and another bright one with 220.1 mJy in 43″ distance. Low resolution catalogues contain only the bright radio source which would lead to high positional deviations and an odd position in the $\alpha_{OX} - \alpha_{RO}$ diagram. With the low flux RX J1456.0+5048 has a typical multifrequency spectrum for a X-ray selected BL Lac object. The absorption features which were used for the redshift determination (Ca H and K and G band) are confirmed by another spectrum with the same telescope.

RX J1458.4+4832 This object is barely visible on the digitized POSS I data. Furthermore the identification of this object is confused by another brighter (B=17.7) starlike object near the X-ray position. A spectrum taken from this object was classified as of stellar spectral type K. For this spectral class the star is too faint to be a plausible optical counterpart. Furthermore the NVSS radio position is only consistent with the position of the BL Lac object.

1ES 1533+535 This object has extremely weak absorption features hardly above the noise level. The red part of the WHT spectrum shows two broad absorption features with a separation consistent with Ca H and K. The blue part of the WHT spectrum shows two neighbouring lines with a position consistent with the MgII doublet and a redshift of $z = 0.89$. Blended together these lines can also be discerned in the Calar Alto 3.5m spectra. No other line could be securely detected at this redshift (in particular the G band). Therefore we consider this redshift as very tentative. This is the highest redshift in the sample, but we have already argued for weak absorption features in high redshift objects. The main conclusions of our paper are not altered if the redshift of this object is considered as unknown. This object is also a member of the *Einstein* Slew Survey.

RX J0832.8+3300 The 4000Å break of this high redshift BL Lac object is comparatively strong.

RX J1237.0+3020 This is another faint object with high redshift. Ca H and K and G band are discernible on the red part of the WHT spectrum, and the MgII doublet can be found as a blend on the Calar Alto 3.5m spectra.